BRL R 1695

BRL

REPORT NO. 1695

SEPARATION AND REATTACHMENT NEAR SQUARE PROTUBERANCES IN LOW REYNOLDS NUMBER COUETTE FLOW

by

Clarence W. Kitchens, Jr.

January 1974

USA BALLISTIC RESEARCH LABORATORIES
ABERDEEN PROVING GROUND, MARYLAND

Destroy this report when it is no longer needed.
Do not return it to the originator.

Secondary distribution of this report by originating or sponsoring activity is prohibited.

Additional copies of this report may be obtained from the National Technical Information Service, U.S. Department of Commerce, Springfield, Virginia 22151.

The findings in this report are not to be construed as an official Department of the Army position, unless so designated by other authorized documents.

B A L L I S T I C R E S E A R C H L A B O R A T O R I E S

REPORT NO. 1695

JANUARY 1974

SEPARATION AND REATTACHMENT NEAR SQUARE PROTUBERANCES IN LOW REYNOLDS NUMBER COUETTE FLOW

Clarence W. Kitchens, Jr.

Exterior Ballistics Laboratory

RDT&E Project No. 1T061101A91A

A B E R D E E N P R O V I N G G R O U N D, M A R Y L A N D

B A L L I S T I C R E S E A R C H L A B O R A T O R I E S

REPORT NO. 1695

CWKitchens,Jr./rt
Aberdeen Proving Ground, Md.
January 1974

SEPARATION AND REATTACHMENT NEAR SQUARE PROTUBERANCES IN LOW REYNOLDS NUMBER COUETTE FLOW

ABSTRACT

Numerical solutions of the steady-state Navier-Stokes equations are obtained which describe flow past a square protuberance immersed in a plane Couette flow. The numerical solutions are illustrated with velocity vector plots, and plots of streamlines and vorticity contours in the flow field for Reynolds numbers between 1 and 200, based on plate velocity and protuberance height. A small separation bubble is predicted upstream of the protuberance with length and height almost independent of Reynolds number. The downstream separation bubble has a height always less than the protuberance height, but a length which increases almost linearly with Reynolds number reaching more than twenty-five protuberance heights at Re = 200. The flow perturbations caused by the protuberance are shown to persist far downstream of the protuberance at Re = 100 and 200.

TABLE OF CONTENTS

LIST OF ILLUSTRATIONS

LIST OF SYMBOLS

h	height of backstep, m
k	height of protuberance, m
u	x-component of velocity, m/sec
v	y-component of velocity, m/sec
x	axial coordinate, m
x_k	position of leading edge of protuberance, m
y	transverse coordinate, m
A	constant for adjusting mesh stretching in equation (15), nondimensional
O	order symbol showing qualitatively the rate at which a limiting value is approached, nondimensional
P	pressure, N/m^2
Re	Reynolds number based on plate velocity and protuberance height $(U_o k/\nu)$, nondimensional
Re_k	local roughness Reynolds number $(U_k k/\nu)$, nondimensional
Re_c	Reynolds number based on centerline pipe velocity and step height $(U_c h/\nu)$, nondimensional
Re_f	Reynolds number based on freestream velocity and step height $(U_f h/\nu)$, nondimensional
U_c	velocity at pipe centerline, m/sec
U_f	freestream velocity at edge of boundary layer, m/sec
U_k	mean velocity that would exist at the protuberance height if the protuberance were not present
U_o	velocity of moving plate in Couette flow, m/sec
X	distance from leading edge of protuberance measured in protuberance heights, $(x-x_k)/k$, nondimensional

δ undisturbed boundary layer thickness, m

ζ vorticity, defined by equation (5), sec^{-1}

λ convergence criterion, nondimensional

μ absolute viscosity, kg/m-sec

ν kinematic viscosity, m^2/sec

ρ density, kg/m^3

ψ stream function, defined by equation (4), m^2/sec

Δy incremental length in y-direction, m

Superscript

n iteration level at which quantity is evaluated

Subscripts

o reference value of stream function or vorticity

p typical point in finite-difference grid

w function evaluated at the wall

D value of function at convex corner D

I. INTRODUCTION

The qualitative features of the flow field downstream of two-dimensional roughness elements immersed in a laminar flat plate boundary layer are well known. In many wind tunnel experiments, such protuberances are employed to promote transition and assure turbulent boundary layer characteristics on models. At high Reynolds number, the flow at the base of the protuberance is separated with the influence of the protuberance persisting downstream for a hundred protuberance heights or more. Sedney[1*] has described the effects of two- and three-dimensional protuberances on boundary-layer flows. In the two-dimensional case at low speeds, transition generally occurs downstream of the reattachment point if the protuberance height k is considerably less than the undisturbed boundary layer thickness δ.

This report describes the flow field near a square two-dimensional protuberance immersed in a plane Couette flow. Numerical solutions are based on a finite-difference analog of the incompressible Navier-Stokes equations. The solution technique is an extension of a method developed by Gosman et al.[2] for the solution of the steady state stream function and vorticity formulation of the Navier-Stokes equations.

The object of this work is to describe the steady flow disturbances created when a two-dimensional protuberance is immersed in a laminar flat plate boundary layer. It should be noted that the boundary layer equations are not valid for describing the flow near the protuberance, but would most likely be applicable far downstream of the reattachment point. In this study a plane Couette flow, an exact solution of the Navier-Stokes equations, is used to model the undisturbed flow on the flat plate. We expect the qualitative features of the separation phenomena induced by the protuberance in the Couette flow to be similar to those found in the flat plate boundary layer case.

Figure 1 shows a schematic of the flow field near a square protuberance immersed in a plane Couette flow. The protuberance is mounted on the stationary bottom plate. The upper plate moves at a constant speed U_0. Far upstream of the protuberance, shown schematically as position 1, the velocity distribution is prescribed by a linear Couette flow profile. As the flow nears the protuberance, we expect it to separate, forming a small upstream recirculation region.

Downstream of the protuberance, at position 2, we expect separated flow profiles with the height of the reversed flow region no larger than the protuberance height k. Velocity profiles at this position will exhibit a velocity overshoot near the moving plate ($u>U_0$) due to the flow constriction caused by the protuberance. Far downstream of the

*References are listed on page 38.

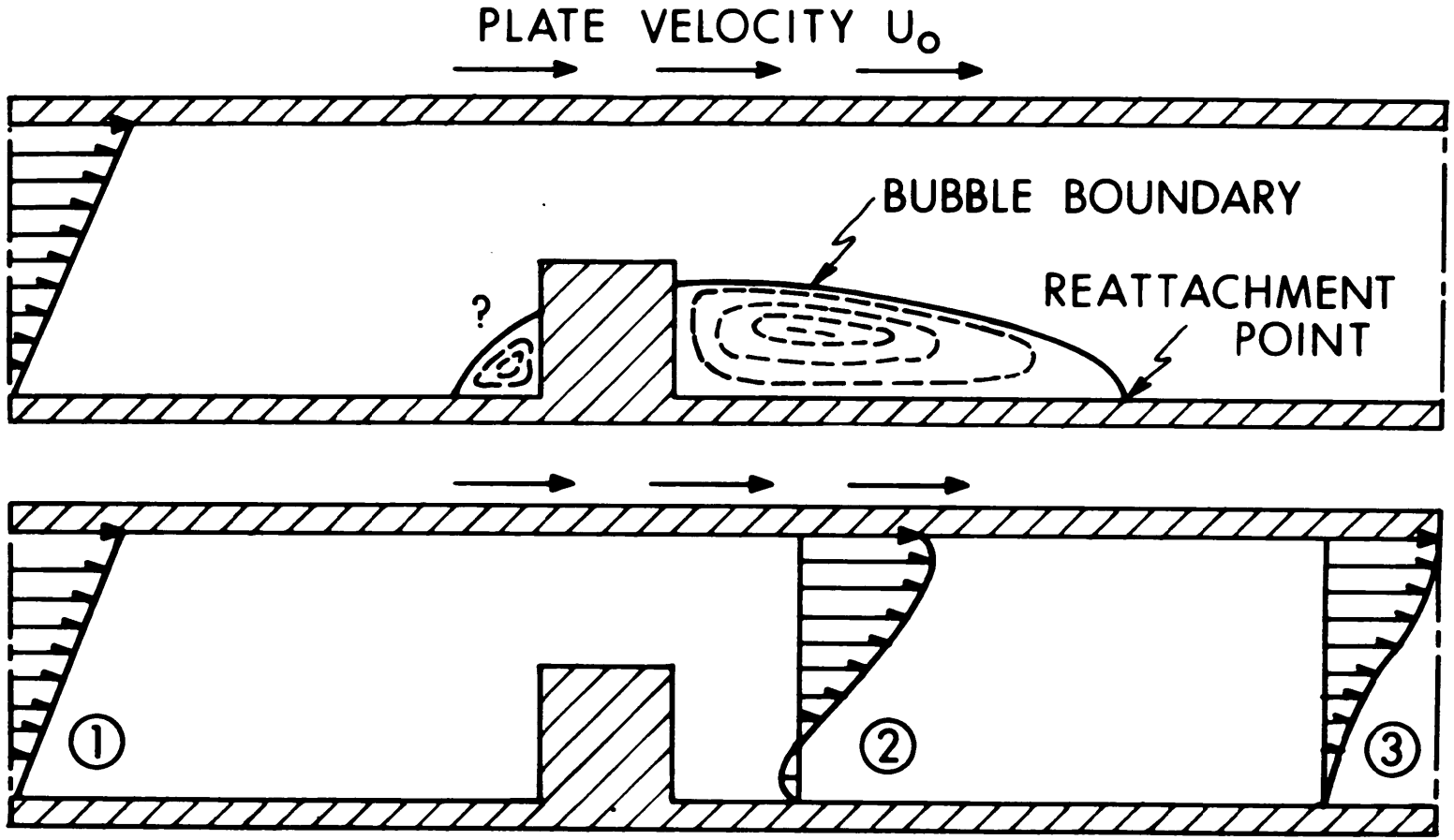

1 – PLANE COUETTE FLOW

2 – SEPARATED FLOW PROFILES WITH VELOCITY OVERSHOOT

3 – "RECOVERING" WAKE PROFILES

Figure 1. Square Protuberance Immersed in Plane Couette Flow

protuberance and the reattachment point, at position 3, the flow still exhibits a perturbation from the original Couette flow. These perturbations decay and the flow returns to the Couette-type distribution farther downstream.

Numerical results are presented which describe the flow near such protuberances for Re = 1, 10, 25, 50, 100 and 200; with the Reynolds number Re based on the plate velocity U_o and the protuberance height k. The local roughness Reynolds number, $Re_k = U_k k/\nu$, is one-half of each of the above values; where U_k is the mean velocity that would exist in the undisturbed flow at the protuberance height if the protuberance was not present. The numerical results are illustrated with CALCOMP plots of streamlines and vorticity contours in the flow field around the protuberance.

II. FORMULATION OF THE PROBLEM

The mathematical description of the disturbed flow near the protuberance should be based on the Navier-Stokes equations because viscous separation phenomena are important. The recirculation region downstream of the protuberance and the position of flow reattachment along the stationary plate influence the length of the recovery zone downstream of the protuberance. In the two-dimensional case, the Navier-Stokes equations can be expressed in rectangular coordinates by the x-momentum equation

$$u\frac{\partial u}{\partial x} + v\frac{\partial u}{\partial y} = -\frac{1}{\rho}\frac{\partial P}{\partial x} + \nu\left(\frac{\partial^2 u}{\partial x^2} + \frac{\partial^2 u}{\partial y^2}\right), \tag{1}$$

and the y-momentum equation

$$u\frac{\partial v}{\partial x} + v\frac{\partial v}{\partial y} = -\frac{1}{\rho}\frac{\partial P}{\partial y} + \nu\left(\frac{\partial^2 v}{\partial x^2} + \frac{\partial^2 v}{\partial y^2}\right). \tag{2}$$

The continuity equation is

$$\frac{\partial u}{\partial x} + \frac{\partial v}{\partial y} = 0. \tag{3}$$

The pressure can be eliminated from the momentum equations by differentiating equation (1) with respect to y, equation (2) with respect to x, and subtracting the resulting equations. The continuity equation (3) can be satisfied by defining the stream function ψ such that

$$u = \frac{\partial \psi}{\partial y} \text{ and } v = -\frac{\partial \psi}{\partial x}. \tag{4}$$

By introducing the definition of vorticity ζ, where

$$\zeta = \frac{\partial v}{\partial x} - \frac{\partial u}{\partial y} ; \tag{5}$$

equations (1), (2) and (3) can be combined with (4) and (5) into two equations: the elliptic vorticity transport equation

$$\frac{\partial}{\partial x}(\zeta\frac{\partial \psi}{\partial y}) - \frac{\partial}{\partial y}(\zeta\frac{\partial \psi}{\partial x}) - \nu(\frac{\partial^2 \zeta}{\partial x^2} + \frac{\partial^2 \zeta}{\partial y^2}) = 0, \tag{6}$$

and an elliptic Poisson-type equation

$$\frac{\partial^2 \psi}{\partial x^2} + \frac{\partial^2 \psi}{\partial y^2} + \zeta = 0. \tag{7}$$

Equations (6) and (7) represent the stream function and vorticity formulation of the Navier-Stokes equations. These equations govern the flow subject to the prescribed boundary conditions. It should be noted that only the prescribed boundary conditions and flow parameters make one numerical solution different from another. The accurate specification of boundary conditions is thus very important. Since these governing equations are elliptic, boundary conditions must be specified on all boundaries of the computational region.

III. BOUNDARY CONDITIONS

Roache[3] discusses many methods for treating boundary conditions for the stream function and vorticity in numerical solutions of the Navier-Stokes equations. It should be noted that many of the methods which have been used in the past to prescribe boundary conditions for the vorticity were inconsistent and/or unsuccessful. The downstream or outflow boundary and the sharp protuberance corners have been particularly troublesome in many instances. The difficulty at the sharp corners will be discussed in detail.

Figure 2 shows an outline of the computational area employed in the numerical calculations and the notation used along boundaries. A plane Couette flow is specified along the upstream boundary AH so that

$$u = U_o(y/2k) \quad \text{and} \quad v = o; \tag{8}$$

with

$$\psi = \int_0^y U_o(\eta/2k)d\eta \text{ and } \zeta = U_o/2k \tag{9}$$

The no slip condition ($u = v = o$) is specified along the stationary plate, AB and EF, and the protuberance, BC, CD and DE. The stream function ψ is specified to be a constant on these boundaries; taken equal to zero for convenience. The vorticity ζ on these boundaries cannot be specified independently of the flow off the surface. Appendix A shows a derivation of the relationship between the vorticity at the

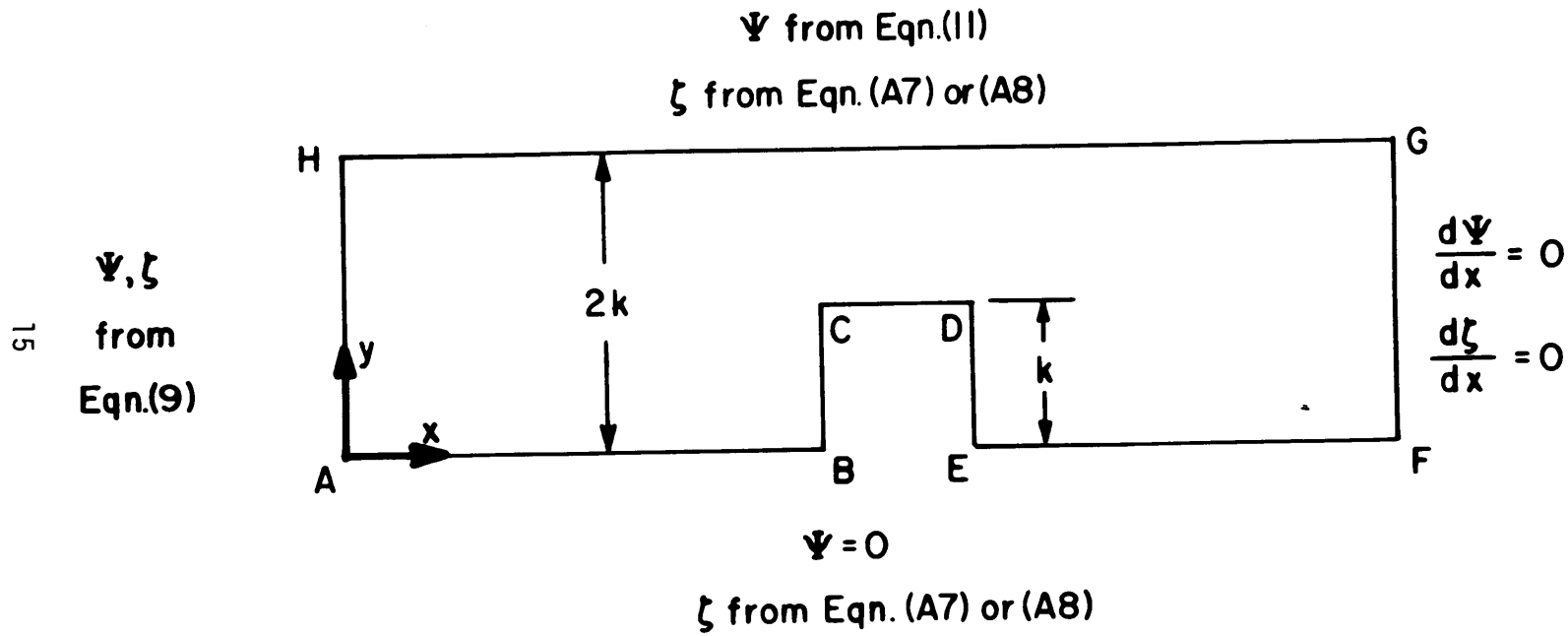

Figure 2. Schematic of Computational Region and Boundary Conditions

wall and the flow adjacent to the wall. Two different expressions for the wall vorticity have been used in obtaining numerical solutions to examine the influence of the wall vorticity equation on the calculated results. These expressions are given by equations (A7) and (A8).

Appendix B describes two alternatives for evaluating the vorticity at the sharp corners, C and D, on the protuberance. The sharp concave corners B and E are no problem because $\zeta = 0$ at these points. In the present difference procedure, the value of ζ at B and E doesn't enter the iteration formulae for nearby points, but its value is needed for vorticity contour plots.

Along the downstream or outflow boundary, FG, the conditions

$$\frac{\partial \psi}{\partial x} = 0 \text{ and } \frac{\partial \zeta}{\partial x} = 0 \tag{10}$$

are specified. The Couette flow solution is one member of the family of profiles that satisfies these boundary conditions. A computational experiment is needed to determine the extent of upstream influence of the errors caused by specifying equations (10) at a fixed position downstream of the protuberance. Results from such tests will be discussed.

The upper plate, GH, moves at a constant velocity U_0. The no slip conditions ($u = U_0$, $v = 0$) are specified along boundary GH. The stream function ψ is thus specified by

$$\psi = U_0 k \tag{11}$$

and the vorticity ζ is determined by using either equation (A7) or (A8).

IV. NUMERICAL PROCEDURE

Gosman et al.[2] describe the complete set of finite-difference equations which were used in this numerical study. The finite-difference representations of equations (6) and (7) are based on the "tank and tube" method. The flow field is divided into an array of cells called tanks which are connected to adjacent cells by tubes. Mass is convected from one cell to another along the tubes. The difference equations are not restricted to evenly spaced nodes and an uneven mesh spacing between grid points can be easily specified by prescribing the x- and y-coordinate of each grid point. An upwind difference scheme is used for the convective terms in the governing equations with information advected into a cell only from cells upwind of it. The finite-difference formulation should therefore be classified as first-order accurate. Gosman[4] has analyzed the difference equations and has concluded that convergence is likely in all circumstances with constant property flow. Divergence of the

iteration procedure has occurred, however, under certain circumstances.[4]

The iteration process used in this study is the Gauss-Seidel procedure. The complete grid is scanned node by node, and the values of ψ and ζ at a particular node are calculated using neighboring values from the previous iteration. Calculations in the first iteration are based on initial guesses for ψ and ζ at all grid points. The scanning process is continued until the grid is completely scanned. Special formulae are necessary on the boundaries. This procedure is then repeated, with each complete scan equal to one cycle of iteration, until the criterion for convergence is satisfied or the calculation is otherwise terminated. If convergence is achieved, the velocity distribution, skin friction coefficient, etc. are calculated and a plot routine is executed.

Convergence is tested by the calculation of the fractional changes

$$\left| \frac{\psi_P^{n} - \psi_P^{n-1}}{\psi_o} \right|_{\text{Maximum in field}} < \lambda, \tag{12}$$

and

$$\left| \frac{\zeta_P^{n} - \zeta_P^{n-1}}{\zeta_o} \right|_{\text{Maximum in field}} < \lambda; \tag{13}$$

where ψ_o and ζ_o are selected reference values of ψ and ζ, typically 0.5 and 1.0, respectively. The value of λ was set at 0.0001 for all calculations. Equations (12) and (13) are applied by calculating the fractional change of ψ and ζ at every grid point in the field for each iteration. When the absolute value of the fractional change is less than λ at every point, convergence is examined in more detail. Care must be taken to examine the convergence of each case because, with the fractional change criteria, a slowly converging process may be mistaken for one that is fully converged. Calculated values of ψ and ζ at selected points in the field are examined over a period of approximately ten iterations to insure that convergence has been achieved if equations (12) and (13) are satisfied. Convergence was not achieved in the calculations for cases with $Re \geq 300$.

V. DESCRIPTION OF NUMERICAL CALCULATIONS

Numerical solutions have been obtained for Re = 1, 10, 25, 50, 100 and 200 which describe the flow around a square protuberance immersed in a plane Couette flow. The iteration procedure used in this study did not converge for cases which were attempted at Re = 300, 500 and 1000. Computational results will be illustrated with selected velocity vector plots, vorticity contours and streamlines in the flow field drawn on an

off-line CALCOMP plotter. A contour plotting subroutine developed by Hartwig[5] was used for interpolation and contour plotting control. Calculations were performed in double precision on the BRLESC I and II computers at the Ballistic Research Laboratories.

Two different grid mesh configurations were used in the calculations. The grid for $Re \leq 50$ consisted of a 6 x 11 cell protuberance immersed in a 51 x 21 cell flow field. The mesh aspect ratio $\beta = \Delta x/\Delta y$ varied from 2.0 near the protuberance to 12.0 at the downstream boundary. Calculations for $Re \geq 100$ were performed using a 6 x 11 cell protuberance immersed in a 81 x 21 cell flow field with β varying from 2.0 near the protuberance to 42.6 at the downstream boundary. The inflow boundary, AH in Figure 2, was located at approximately X = -8.0, where

$$X = (x-x_k)/k \tag{14}$$

refers to distances measured from the position of the protuberance leading edge, x_k, in terms of the protuberance height k.

The outflow boundary, FG, was located at approximately X = 9.5 in the 51 x 21 grid and at approximately X = 93.5 in the 81 x 21 grid. The mesh spacing in the y-direction was fixed at $\Delta y = k/10$. The mesh spacing in the x-direction varied from $\Delta x = k/5$ near the protuberance to $\Delta x = (1.2)k$ at the outflow boundary in the 51 x 21 grid and to $\Delta x = (4.3)k$ at the outflow boundary in the 81 x 21 grid. The mesh spacing downstream of the protuberance was stretched according to

$$X_{i+1} = X_i + k/5 + \frac{|\tan(iA/10)|}{2\tan(A)}\ ; \tag{15}$$

where A = 1.0 and i = 1,2,··10 in the 51 x 21 grid, and A = 0.05 and i = 1,2,··40 in the 81 x 21 grid.

Figure 3 shows a velocity vector plot of the flow around the protuberance at Re = 1. The location of grid points in the 51 x 21 grid can be visualized in this figure--a grid point is located at the tail of each velocity vector. The magnitude of the plate velocity U_o is shown by the length of the vectors above the moving plate. All vectors are scaled with respect to U_o. This plot shows that at very low Re the flow disturbances caused by the protuberance are confined to a zone within a few protuberance heights on either side of the protuberance. The flow returns to an exact Couette flow distribution by X = 9.0; thus flow disturbances are confined to a zone very near the protuberance at Re = 1.

Figure 4 shows vorticity contours and streamlines in the protuberance flow field for Re = 1. The flow conditions are the same in Figures 3 and 4. The arrows shown above the moving plate in the streamline and vorticity contour plots are not plotted to the same scale as in the velocity vector plots. The numerical treatment of the boundary

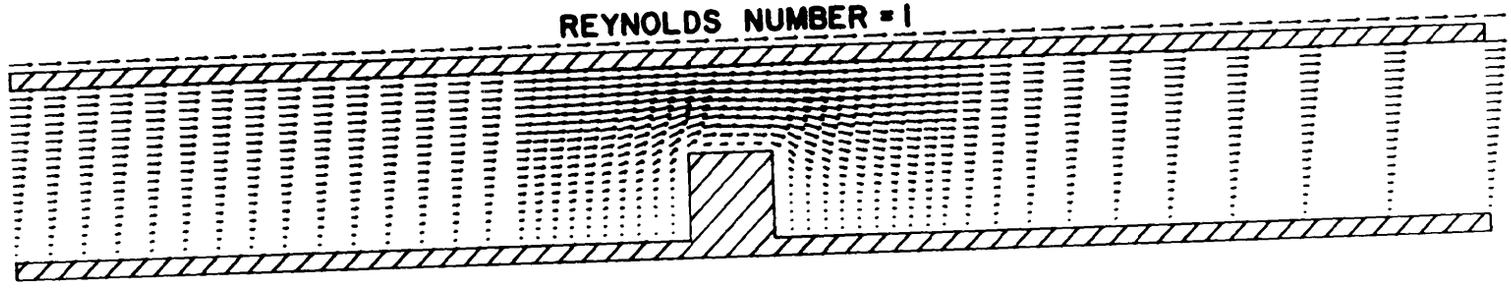

Figure 3. Flow Field Velocity Vectors for Re = 1 with Second-Order Double-Valued Corner Vorticity

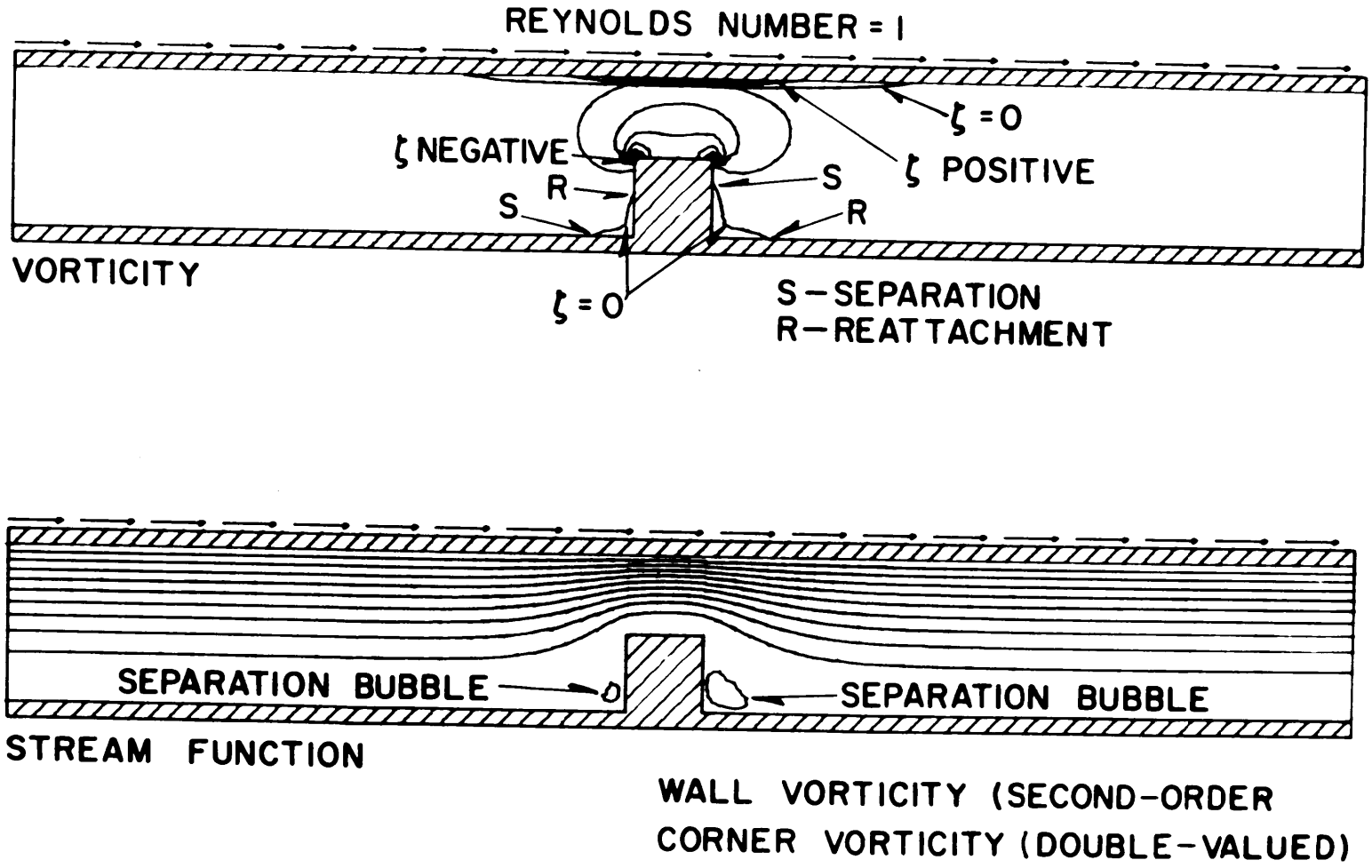

Figure 4. Streamlines and Vorticity Contours for Re = 1

conditions for each case is indicated below the contour plots. Figure 4 represents results obtained using a second-order formulation for the wall vorticity given by equation (A8), treating the vorticity at the sharp convex corners using the double-valued method described in Appendix B.

Figure 4 shows that at Re = 1, the flow field is nearly symmetric about the mid-plane of the protuberance, X = 0.5. We expect flow field symmetry in the Stokes flow limit as Re→0. Eleven streamlines are plotted in the non-recirculating flow region in all cases which will be discussed. It should be remembered that the upper plate is one streamline and the lower plate and protuberance is another. The difference in stream function between two adjacent streamlines is specified so that

$$\Delta\psi = \frac{\psi_{\text{upper plate}} - \psi_{\text{lower plate}}}{10}\ ; \tag{16}$$

where $\Delta\psi$ is proportional to the mass flow rate per unit area between two adjacent streamlines. Figure 4 shows that the mass flow rate between the bottom plate and the adjacent streamline is much lower than between any other two adjacent streamlines, as a consequence of the low flow velocities near the stationary plate.

Streamlines in the separation bubbles upstream and downstream of the protuberance have negative values of ψ, with $|\psi|$ very small. A different $\Delta\psi$ spacing is used in these regions, depending on the strength of the recirculation. Either one or as many as four streamlines are plotted in the separation bubbles depending on the magnitude of ψ.

For the case shown in Figure 4, the downstream separation bubble consisted of three grid points with negative values of stream function. The plotting routine denoted this with a single closed contour as indicated in the figure. The upstream separation bubble, on the other hand, was much smaller--consisting of a single grid point with negative ψ. Since the apparent size of the separation bubble depends on the ψ-contour plotted, the location of separation and reattachment should be determined from the vorticity contours for $\zeta = 0$.

Vorticity contours in the flow field for Re = 1 are also shown in Figure 4. Negative values of vorticity are plotted with

$$\Delta\zeta = \frac{\zeta_{\text{max. negative value in field}}}{7} \tag{17}$$

between adjacent vorticity contours. The closely spaced contours near the protuberance convex corners indicate large vorticity gradients at these points. Positive values of vorticity, indicating counter-clockwise rotation of fluid elements, are found adjacent to the moving plate. Four vorticity contours are plotted in this region with

$$\Delta\zeta = \frac{\zeta_{\text{max. positive value in field}}}{3} \tag{18}$$

between adjacent contours.

As can be shown, points of zero vorticity along the stationary plate and protuberance surface correspond to points of flow separation and reattachment. The sharp concave corners at the protuberance-plate intersection are also points with vorticity equal zero. The situation on the moving plate is different. Points along the moving plate with vorticity zero do not indicate the position of separation or reattachment as can be shown from equation (A7). A contour for $\zeta = 0$ is plotted near the moving plate, separating the contours for ζ positive from those for ζ negative. Contours connecting points of zero vorticity are plotted in Figure 4 and can be used to locate points of separation and reattachment by comparing these contours with the separated flow streamlines. The predicted location of separation and reattachment depends on the method used to treat the vorticity boundary conditions.

Calculations for Re = 10 illustrate the influence of the vorticity boundary conditions on the numerical solution. Figure 5 shows streamlines and vorticity contours for Re = 10 using the second-order formulation for wall vorticity (A8) and the double-valued treatment at the convex corners. The upstream separation bubble is seen to be slightly smaller than at Re = 1, with the downstream separation bubble much larger. Reattachment of the downstream separation bubble occurs at approximately X = 3.0.

The numerical solution depicted in Figure 5 shows an inconsistency near the separation point on the downstream protuberance face. If separation is defined to occur where $\zeta = 0$, then separation occurs less than one cell below the downstream corner. If separation is defined by extrapolating the dividing streamline back to the downstream protuberance face, then separation occurs approximately one and one-half cells below the corner. This inconsistency is not present in the cases for higher Reynolds numbers and at Re = 10 it occurs only when the double-valued vorticity method is used at the sharp convex corners. It thus appears that for the case shown in Figure 5 we can infer only an approximate position of separation, namely about (0.1)k below the downstream corner.

Figure 6 shows that the results for Re = 10 are practically unchanged if the first-order formulation for wall vorticity (A7) is employed instead of the second-order formulation used in Figure 5. The inconsistency in the separation point location is still present with separation approximately (0.1)k below the downstream corner.

The positions of separation and reattachment are shifted slightly for Re = 10 if the single-valued method for corner vorticity is used instead of the double-valued method. The single-valued method biases the results toward separation at the sharp corner. Figure 7 shows that separation occurs within the first cell below the corner, with no inconsistency using ψ and ζ to locate separation. Reattachment now occurs farther downstream at X = 3.2.

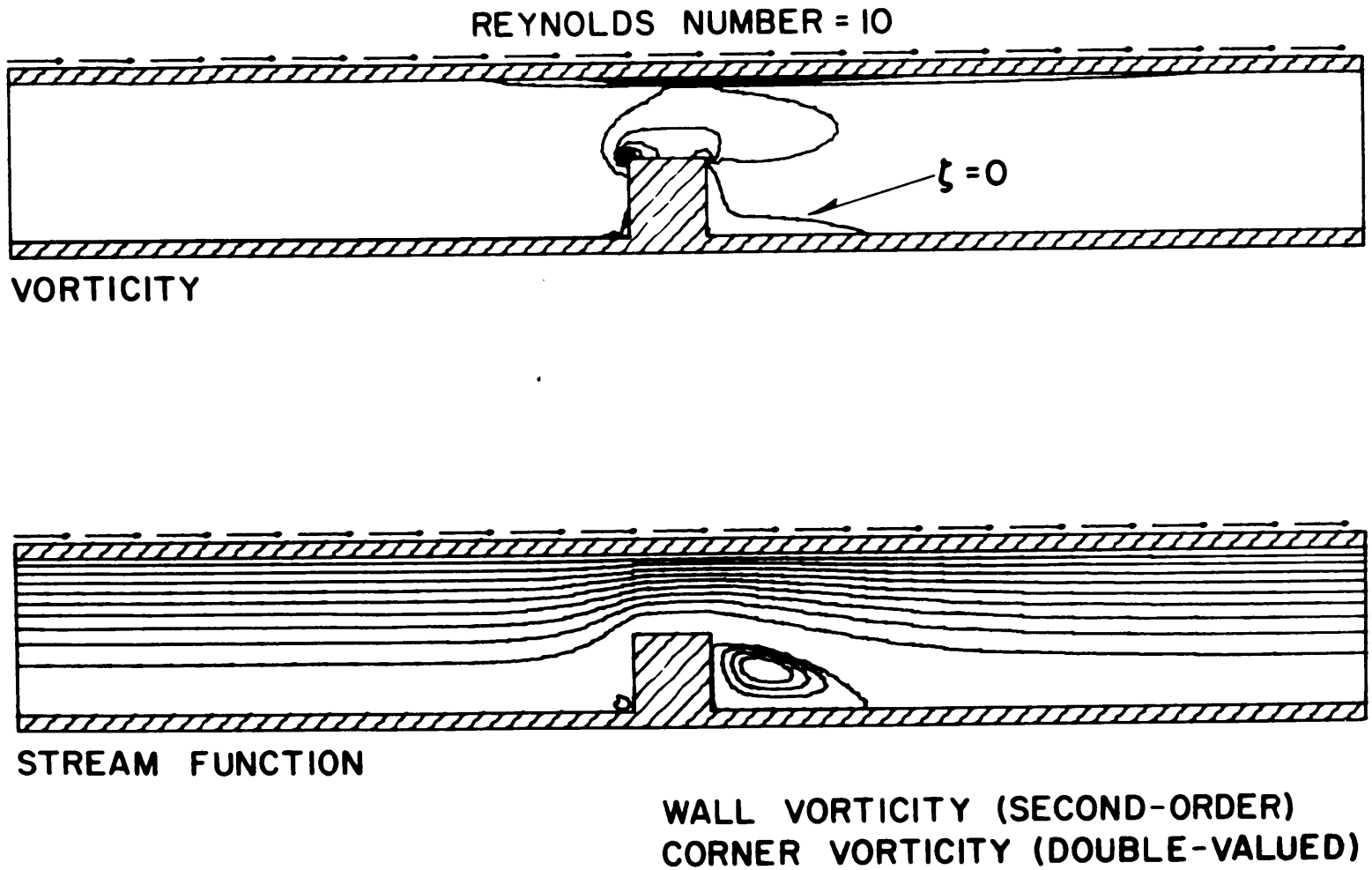

Figure 5. Contour Plots for Re = 10 with Second-Order Double-Valued Corner Vorticity

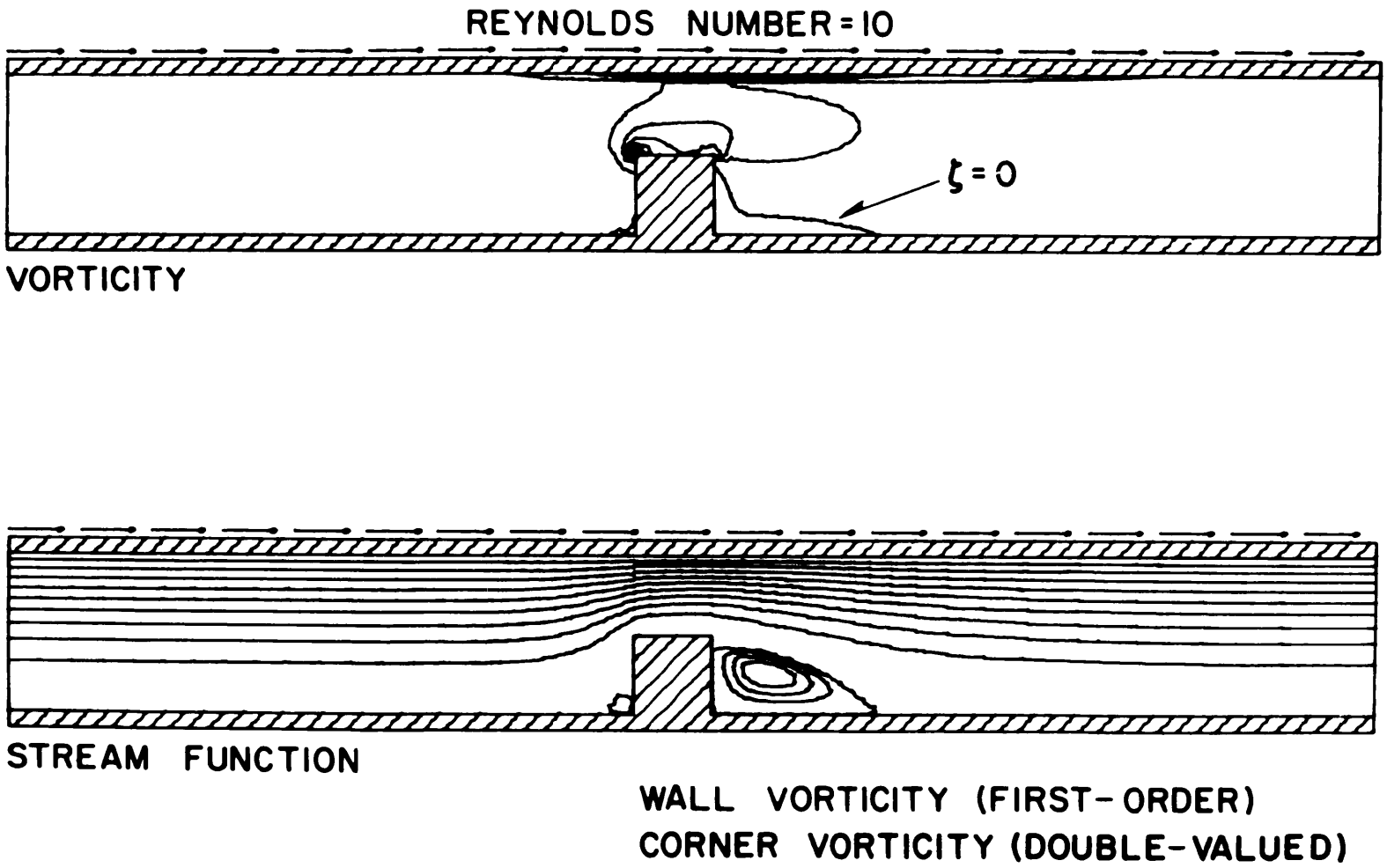

Figure 6. Contour Plots for Re = 10 with First-Order Double-Valued Corner Vorticity

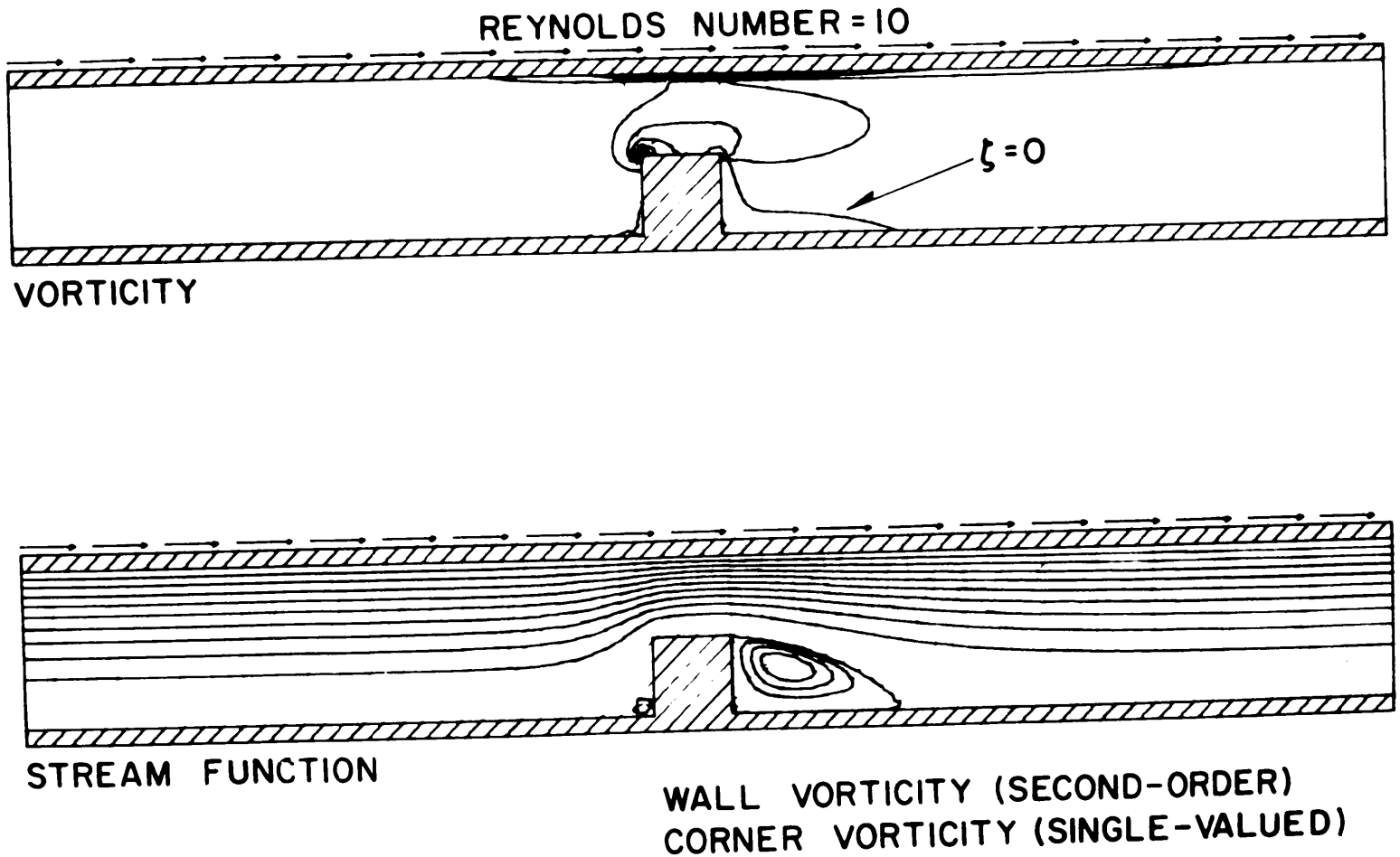

Figure 7. Contour Plots for Re = 10 with Second-Order Single-Valued Corner Vorticity

Figure 8 shows that the position of downstream separation changes slightly if the first-order formulation for wall vorticity (A7) is used instead of second-order formulation shown in Figure 7. The position of reattachment remains at X = 3.2. Comparison of Figures 7 and 8 shows that the prediction of the upstream separation bubble is affected slightly by the order of accuracy used in calculating the wall vorticity.

It is interesting to note that in spite of the small changes caused by the four different boundary conditions, the general features of the predicted flow fields are similar. The upstream separation bubble is very small--less than (0.5)k in height and length. The downstream separation bubble has a height no greater than the protuberance height and a length equal to approximately two protuberance heights at Re = 10. As has been shown, the locations of separation and reattachment cannot be resolved precisely because of the uncertainty about the boundary conditions.

Figure 9 shows streamlines and vorticity contours in the flow field for Re = 25 based on the second-order formulation for wall vorticity and the double-valued technique at the corners. The upstream separation bubble is very small--approximately (0.3)k high based on the $\zeta = 0$ contour. The downstream separation bubble is almost (4.15)k long at this Reynolds number. It appears that as the Reynolds number increases, the predicted location of downstream separation is not as sensitive to the vorticity boundary conditions as at Re = 10. There is no inconsistency in locating the position of downstream separation at Re = 25. Separation occurs less than one cell below the downstream corner. Calculations were performed for Re = 25 using other wall vorticity boundary conditions but the results differ only slightly from those shown in Figure 9.

Figure 10 shows velocity vectors in the flow field for Re = 50. As discussed previously, a velocity overshoot occurs adjacent to the moving plate due to the flow constriction. U-components as large as $(1.44)U_o$ are present in the flow field at Re = 50. Figure 10 shows that appreciable flow disturbances exist at the downstream boundary located at X = 9.5. It is expected that the x-wise decay of these disturbances could be predicted if the grid points were continued beyond the present downstream boundary. The recovery zone may extend, however, for several hundred protuberance heights.

Figure 11 shows streamlines and vorticity contours in the flow field for Re = 50. These plots are based on a numerical solution using the second-order formulation for the wall vorticity and the double-valued vorticity technique at the convex corners. A very small separation bubble is predicted upstream of the protuberance. The flow separates less than one cell below the downstream corner and reattaches at X = 8.2.

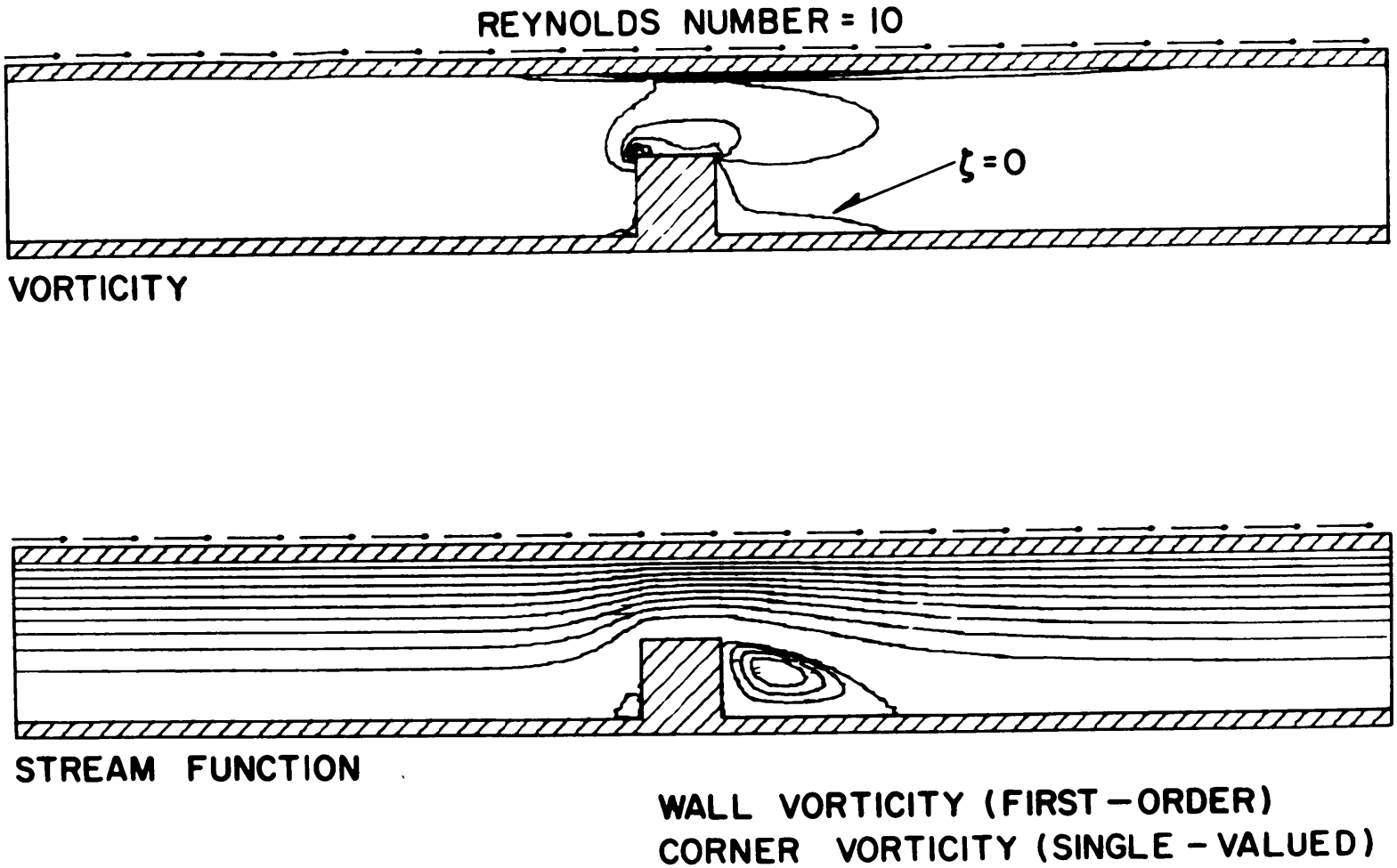

Figure 8. Contour Plots for Re = 10 with First-Order Single-Valued Corner Vorticity

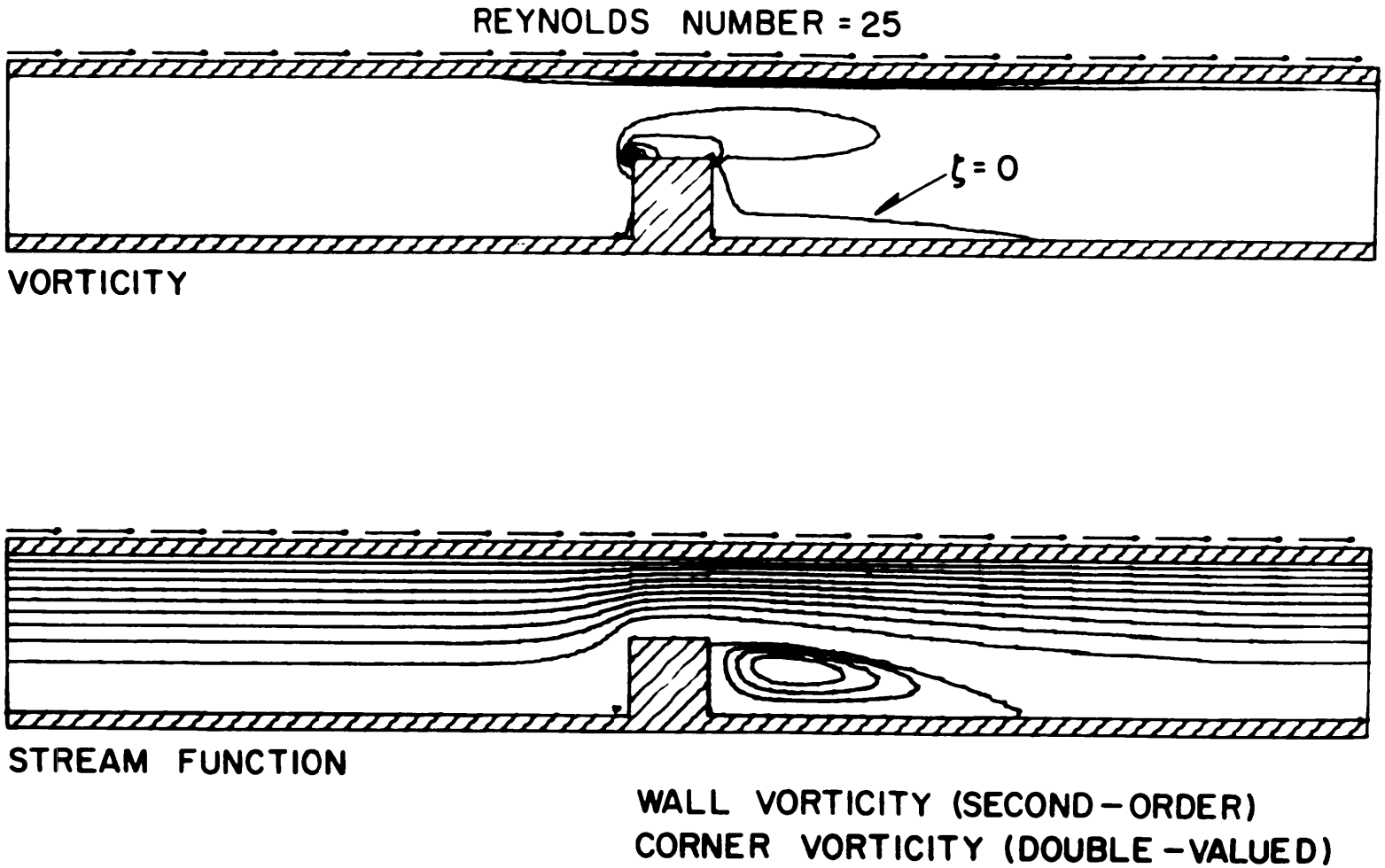

Figure 9. Contour Plots for Re = 25 with Second-Order Double-Valued Corner Vorticity

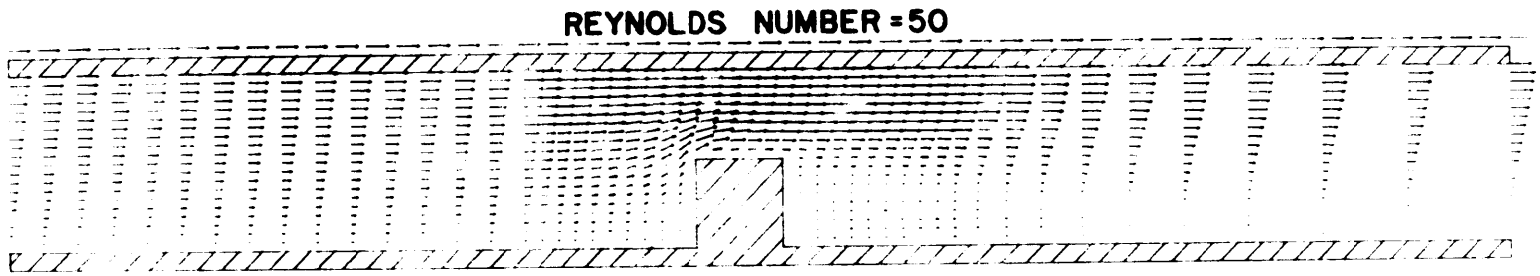

Figure 10. Flow Field Velocity Vectors for Re = 50 with Second-Order Double-Valued Corner Vorticity

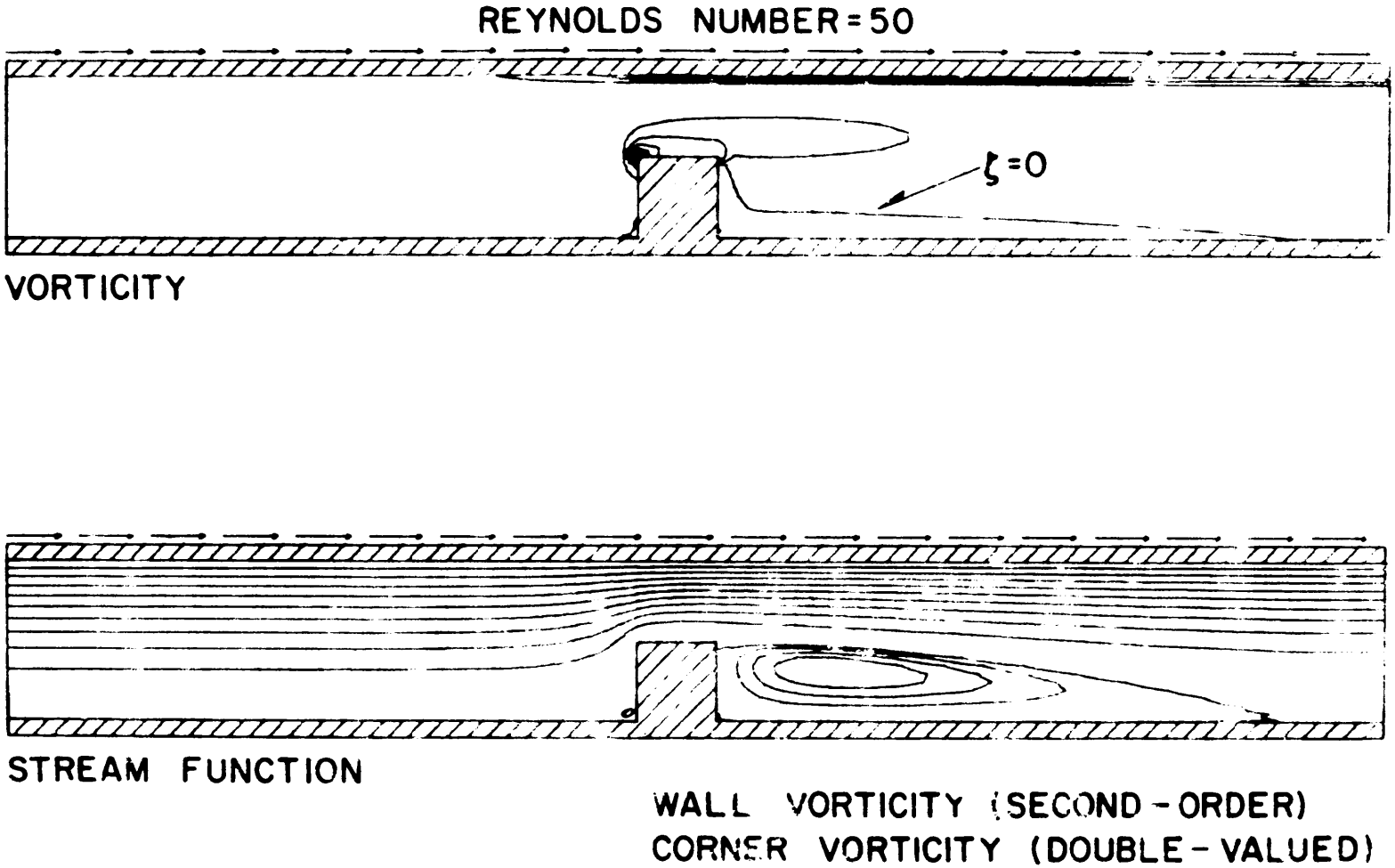

Figure 11. Contour Plots for Re = 50 with Second-Order Double-Valued Corner Vorticity

A computational test was performed to determine the influence of the downstream boundary position on the results shown in Figure 11. The downstream boundary in Figure 11 is at X = 9.5. This boundary was moved farther downstream to approximately X = 14.0 and the calculation for Re = 50 was repeated. There was no change in the results to the scale of the contour plots shown in Figure 11.

A computational test was also performed to determine the influence of the inflow boundary position on the results shown in previous figures. The inflow boundary was placed at X = -4.0 and calculations for Re = 10, 25 and 50 were repeated. The results near the protuberance only changed slightly, but it was evident that perturbations caused by the presence of the protuberance were affecting the calculations for grid points adjacent to the inflow boundary; i.e. grid points next to the inflow boundary no longer showed an exact Couette flow behavior. With the inflow boundary at X = -8.0 the exact Couette flow solution is predicted for the entire region between the inflow boundary and X = -4.0 for Re = 50.

Calculations for Re>50 were performed using the larger 81 x 21 grid to accommodate the large separated flow region expected at higher Reynolds numbers. The downstream boundary was located at X = 93.5. Figure 12 shows streamlines and vorticity contours in part of the flow field for Re = 100. Separation occurs less than one cell below the downstream corner with reattachment at X = 14.2. The calculations predict that the flow disturbances introduced by the protuberance have not fully decayed at X = 93.5. Perturbations of the x-component of local velocity as large as 0.44% of the Couette flow value at the same position above the stationary plate are present at X = 93.5. The largest perturbations are found adjacent to the stationary plate--one cell height off the plate.

Figure 13 shows streamlines and vorticity contours in part of the flow field for Re = 200. Separation occurs less than one cell below the downstream corner with reattachment at X = 26.0. At Re = 200 the flow disturbances introduced by the protuberance decay more slowly than at Re = 100. At Re = 200 perturbations of the x-component of local velocity as large as 8.1% of the Couette flow value at the same y-position are present at X = 93.5. The calculation for Re = 200 required 382 iterations, using crude initial guesses, to satisfy the fractional change criteria given by equations (12) and (13). This required approximately 31 minutes of computer time on BRLESC. Cases for lower Reynolds numbers required less computer time and fewer iterations for convergence using the same initial guesses.

Cases for Re = 300, 500 and 1000 were run, but convergence was not achieved for any of these cases in 500 iterations. In these cases the predicted values of stream function and vorticity at a given point in the flow began to fluctuate, with no apparent pattern toward convergence, after approximately 400 iterations. Each case was run for 500 iterations

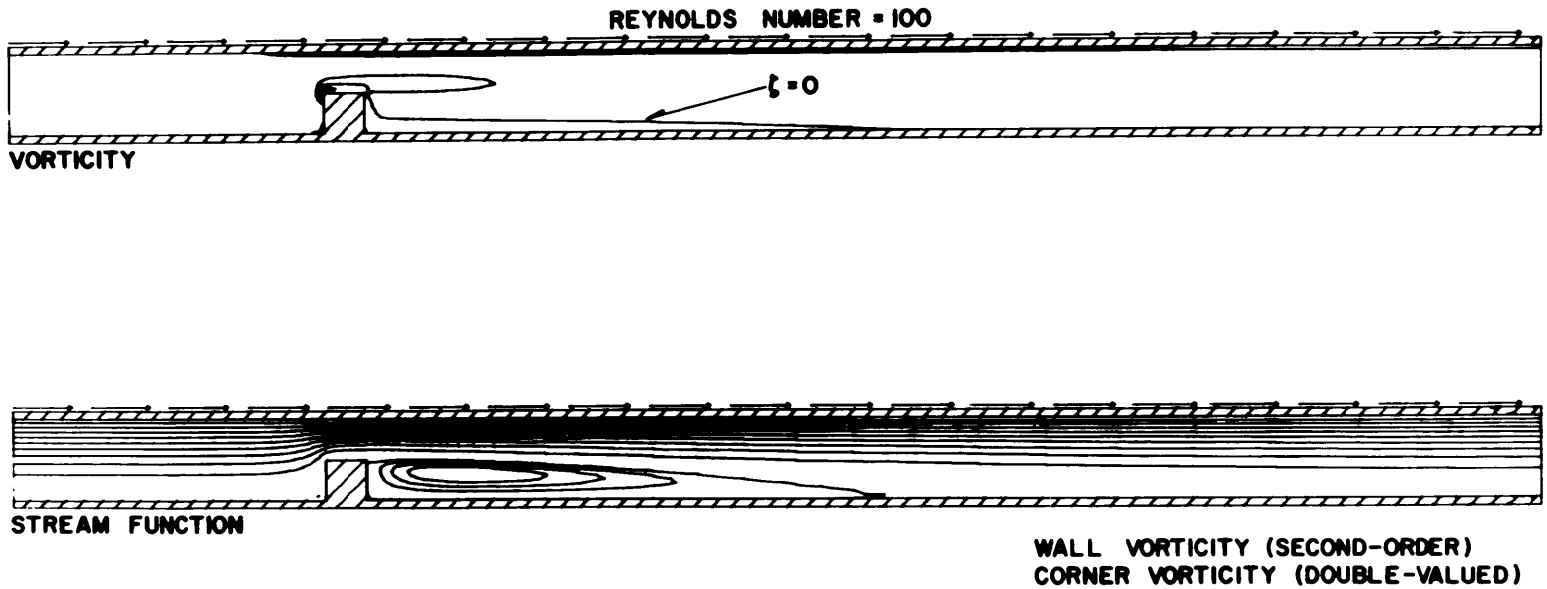

Figure 12. Streamlines and Vorticity Contours Near Protuberance for Re = 100

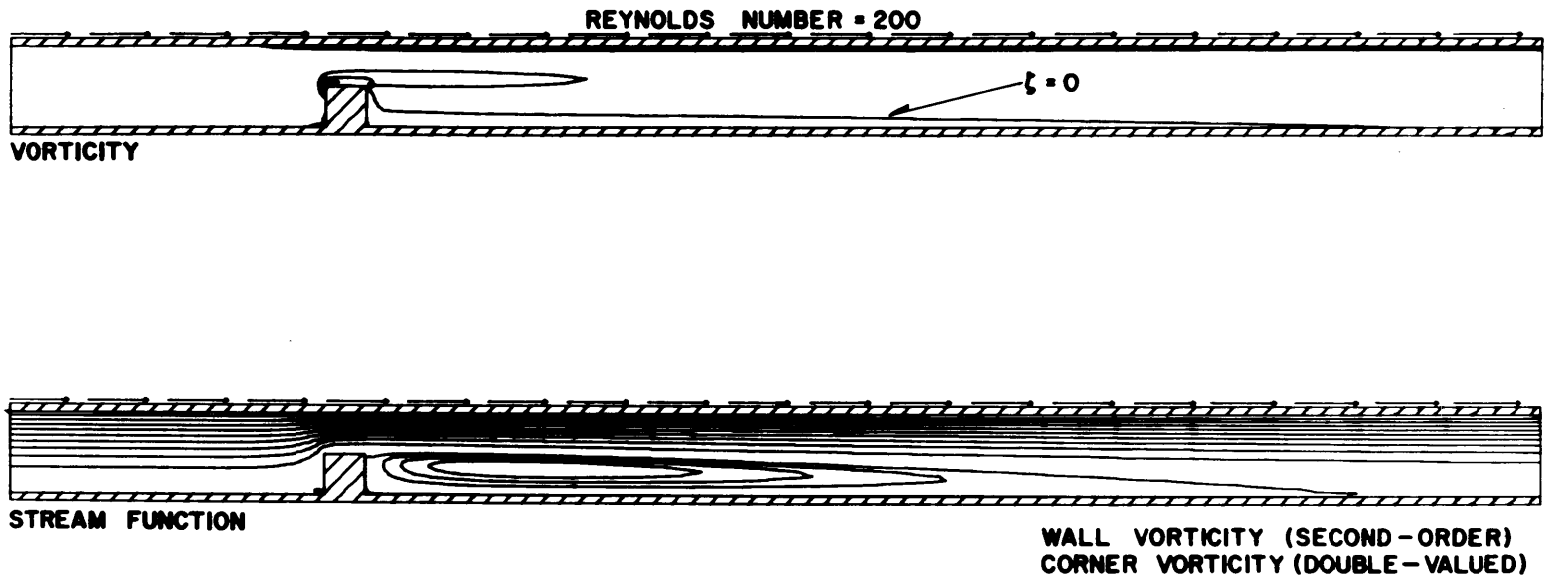

Figure 13. Streamlines and Vorticity Contours Near Protuberance for Re = 200

and then terminated for non-convergence. The reasons for non-convergence could not be determined. It is interesting to recall the experiences of Macagno and Hung[6] and Mueller and O'Leary[7] in related problems.

Macagno and Hung[6] studied the flow of a liquid through an axisymmetric conduit expansion by numerical calculations and used experimental results to verify their calculations. Their computational simulation was based on two different approaches. The first involved an iterative numerical scheme for the steady flow equations, similar to the approach used in the present study. Their second approach was based on the equations for unsteady flow, retaining the local acceleration terms. Their results show the steady-state iterative procedure becomes "unstable" as the Reynolds number is increased. We discuss their results in terms of a Reynolds number, Re_c, based on the step height and the centerline velocity in the smaller upstream pipe. They succeeded in using the iterative steady flow approach for $Re_c<100$ and the results were in agreement with results based on the unsteady equations. Their results for Re_c = 100 and 200 are based on the unsteady approach because ". . . for the same mesh size, the steady approach would have been unstable."

Calculations of laminar flow over a two-dimensional backstep by Mueller and O'Leary[7] were performed using an explicit finite-difference form of the unsteady equations. Their Reynolds number Re_f is based on the freestream velocity and step height. They compare their numerical results with experimental data for $Re_f \leq 100$ and present numerical results for Reynolds numbers as large as Re_f = 200. They experience no computational instabilities in these cases. Their experimental work, however, shows that for $Re_f>100$, ". . . three-dimensional effects appear just before reattachment in the form of helical motion. The recirculation center then appears to become increasingly unstable and eventually appears to break up into several small center eddies. The flow, possibly because of three-dimensional effects and/or with the onset of vortex shedding, is increasingly unstable as the Reynolds number is raised."

The convergence problems which were experienced in the present study for Re>200 are probably related to the stability problems discussed by Macagno and Hung[6]. The grid spacing Δx in our 81 x 21 grid becomes very large downstream of the protuberance with $\Delta x/k$ as large as 4.26 at X = 93.5. It is also possible, however, that our convergence problems are related to a physical flow unsteadiness of the type described by Mueller and O'Leary[7] in their experiments for $Re_f>100$. This intriguing question cannot be resolved in the present numerical study.

VI. DISCUSSION AND CONCLUSIONS

The flow around a square protuberance immersed on a plane Couette flow has been studied by computational simulation for Reynolds numbers up to 200. The numerical solutions predict a very small separated flow region upstream of the protuberance with length and height practically independent of Re. The downstream separation bubble, on the other hand, has a height of order k and a length which increases almost linearly with Reynolds number.

Figure 14 shows that the position of reattachment of the downstream separation bubble varies almost linearly with Reynolds number according to the numerical calculations. Two sets of experimental data for backstep-type flows are shown for comparison. Measurements by Macagno and Hung[6] for an axisymmetric conduit expansion are plotted against Re_c, based on the centerline velocity and step height. Measurements by Mueller and O'Leary[7] for flow over a two-dimensional backstep are plotted in terms of Re_f, based on the freestream velocity and step height. Klebanoff and Tidstrom[8] (not shown in Figure 14) found reattachment at X between 30 and 40 for a cylindrical rod in a flat plate boundary layer. Their experimental results are for Reynolds numbers between 550 and 916 based on protuberance height and freestream velocity. Unfortunately, it is not possible to compare our numerical results in a quantitative sense with any of these experimental measurements because of the difference in geometries. It does appear, however, that the separated flow region downstream of a square protuberance may be significantly longer than that found in the backstep type geometry at comparable Reynolds numbers.

The present results predict that the flow disturbances introduced by the protuberance decay more slowly as the Reynolds number increases. Significant velocity perturbations are found at X = 93.5 in our calculations for Re = 200. These perturbations tend to decrease the skin friction along the plate downstream of the protuberance from the value that would exist in the undisturbed flow.

The difficulties in treating the boundary conditions for vorticity at the sharp protuberance corners have been discussed. Results for Re = 10 have shown that it is not possible to resolve the exact location of separation on the downstream protuberance face. Numerical results for $Re \geq 25$ predict separation to occur less than one cell below the downstream corner. Calculations for a two-dimensional backstep geometry by Mueller and O'Leary[7] also predicted separation below the corner so they investigated the location of separation in their experiments; they remark, ". . . although suggested in some photographs, separation below the corner could not clearly be seen." It thus seems appropriate to interpret our numerical prediction of separation less than one cell below the corner for $Re \geq 25$ as separation at the corner itself within the accuracy of the finite-difference calculation.

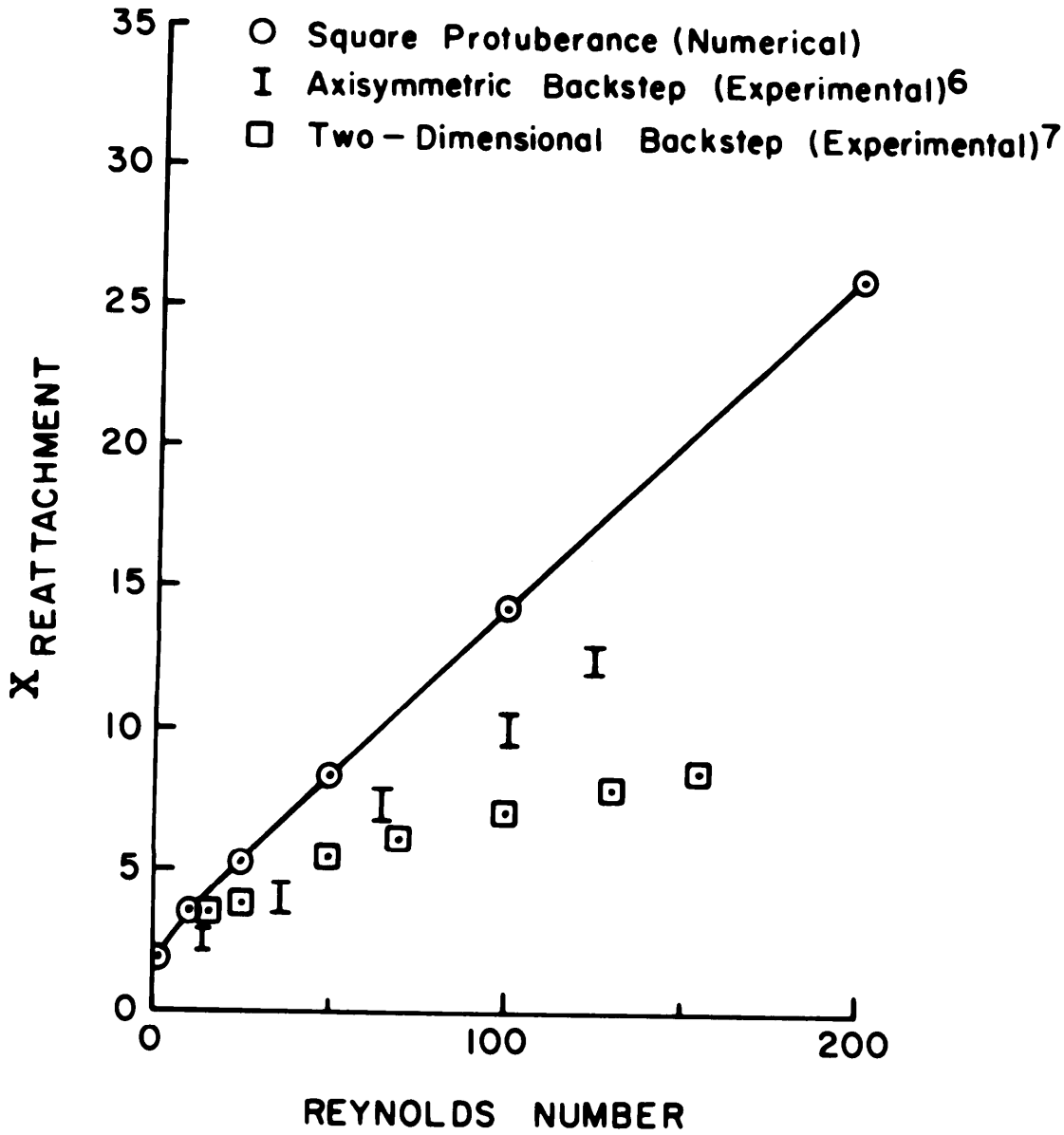

Figure 14. Variation of Downstream Reattachment Position with Reynolds Number

ACKNOWLEDGEMENT

The author acknowledges with thanks the encouragement and helpful comments received from Dr. Raymond Sedney.

REFERENCES

1. R. Sedney, "A Survey of the Effects of Small Protuberances on Boundary-Layer Flows," AIAA J., Vol. 11, No. 6, June 1973, pp. 782-792.

2. A. D. Gosman, W. M. Pun, A. K. Runchal, D. B. Spalding, and M. Wolfshtein, Heat and Mass Transfer in Recirculating Flows, London, Academic Press, 1969.

3. P. J. Roache, Computational Fluid Dynamics, Albuquerque, New Mexico, Hermosa Publishers, 1972.

4. Private Communication from A. D. Gosman, Imperial College of Science and Technology, London, August 1972.

5. G. W. Hartwig, Jr., "CONTUR - A FORTRAN IV Subroutine for the Plotting of Contour Lines," BRL Memorandum Report 2282, March 1973.

6. E. O. Macagno and T. K. Hung, "Computational and Experimental Study of Captive Annular Eddy," J. Fluid Mech., Vol. 28, Part 1, 1967, pp. 43-64.

7. T. J. Mueller and R. A. O'Leary, "Physical and Numerical Experiments in Laminar Incompressible Separating and Reattaching Flows," AIAA Paper 70-763. Presented at the AIAA 3rd Fluid and Plasma Dynamics Conference, Los Angeles, June 1970.

8. P. S. Klebanoff and K. D. Tidstrom, "Mechanism By Which a Two-Dimensional Roughness Element Induces Boundary Layer Transition," The Physics of Fluids, Vol. 15, No. 7, July 1972, pp. 1173-1188.

9. P. J. Roache and T. J. Mueller, "Numerical Solutions of Laminar Separated Flows," AIAA J., Vol. 8, No. 3, March 1970, pp. 530-538.

APPENDIX A

The proper boundary conditions for viscous flow along a moving or fixed wall are the "no slip" conditions. If vorticity is used as a dependent variable in a numerical solution, then relations between the vorticity at points along the wall and the flow adjacent to the wall must be used in the calculation which are consistent with the "no slip" conditions. More than one equation for the wall vorticity can be derived depending on the truncation error that can be tolerated.

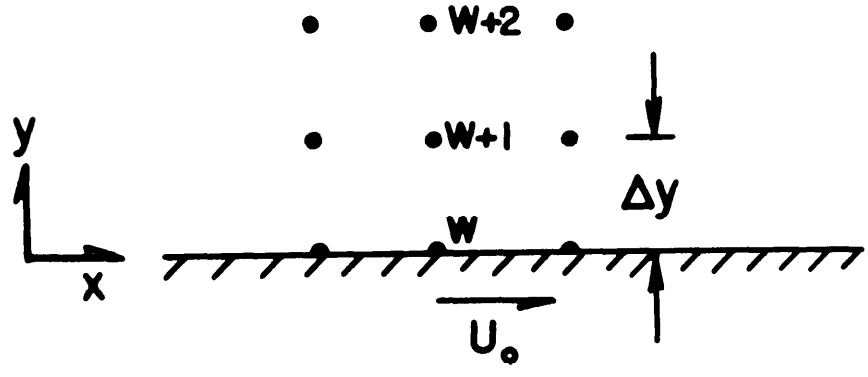

Figure A-1 Grid Notation for Vorticity Boundary Conditions at Wall

Consider a wall moving at constant speed U_o shown in Figure A-1. The relations which will be derived are also valid for a fixed wall when U_o is set equal to zero. We expand the stream function ψ to ψ_{w+1} by a Taylor series expansion out from the wall value ψ_w such that

$$\psi_{w+1} = \psi_w + (\Delta y)\frac{\partial \psi}{\partial y}\Big|_w + \frac{(\Delta y)^2}{2}\frac{\partial^2 \psi}{\partial y^2}\Big|_w + \frac{(\Delta y)^3}{6}\frac{\partial^3 \psi}{\partial y^3}\Big|_w + O(\Delta y^4). \qquad (A1)$$

The terms in equation (A1) can be rewritten by using the "no slip" conditions

$$u_w = U_o \quad \text{and} \quad v_w = 0, \qquad (A2)$$

the definition of stream function

$$u = \frac{\partial \psi}{\partial y} \quad \text{and} \quad v = -\frac{\partial \psi}{\partial x}, \qquad (A3)$$

and the definition of vorticity

$$\zeta = \frac{\partial v}{\partial x} - \frac{\partial u}{\partial y} . \tag{A4}$$

The vorticity at the wall can be expressed as the second derivative

$$\zeta_w = - \frac{\partial^2 \psi}{\partial y^2}\Big|_w \tag{A5}$$

by combining equations (A2), (A3) and (A4). Equation (A1) can be rewritten as

$$\psi_{w+1} = \psi_w + (\Delta y)U_o - \frac{(\Delta y)^2}{2} \zeta_w - \frac{(\Delta y)^3}{6} \left[\frac{\zeta_{w+1} - \zeta_w}{\Delta y}\right] + O(\Delta y^4). \tag{A6}$$

Equation (A6) yields different equations for the wall vorticity depending on the order of truncation of the Taylor series. The lowest-order accurate equation results from retaining terms up to order $(\Delta y)^2$ in equation (A6) and solving for ζ_w

$$\zeta_w = - \frac{2}{(\Delta y)^2} [\psi_{w+1} - \psi_w - (\Delta y)U_o] + O(\Delta y). \tag{A7}$$

Equation (A7) represents the first-order formulation for the wall vorticity. The second-order formulation

$$\zeta_w = - \frac{3}{(\Delta y)^2} [\psi_{w+1} - \psi_w - (\Delta y)U_o] - \frac{\zeta_{w+1}}{2} + O(\Delta y^2) \tag{A8}$$

is obtained by retaining terms up to order $(\Delta y)^3$ in equation (A6).

Expressions for the wall vorticity ζ_w can be derived in a similar manner having higher-order accuracy. Since the finite-difference equations used for interior points are only first-order accurate, equation (A8) should be of sufficient accuracy. It should be noted that when $\zeta_{w+1} \neq \zeta_w$ equations (A7) and (A8) give two different approximations to the wall vorticity. If (Δy) is used to represent the grid spacing normal to the wall, then equations (A7) and (A8) remain the same regardless of the wall orientation or the value of ψ on the wall. Computational results will be used to illustrate the effects of using these two different expressions for wall vorticity.

APPENDIX B

The description of the wall vorticity at the concave protuberance corners, B and E in Figure B-1, presents no difficulty because $\zeta = 0$ at these points. The specification of vorticity boundary conditions at the sharp convex protuberance corners, C and D, poses a difficult computational dilemma. A certain type of non-uniqueness occurs at these two corners because there are several alternatives available for evaluating the wall vorticity at these points.

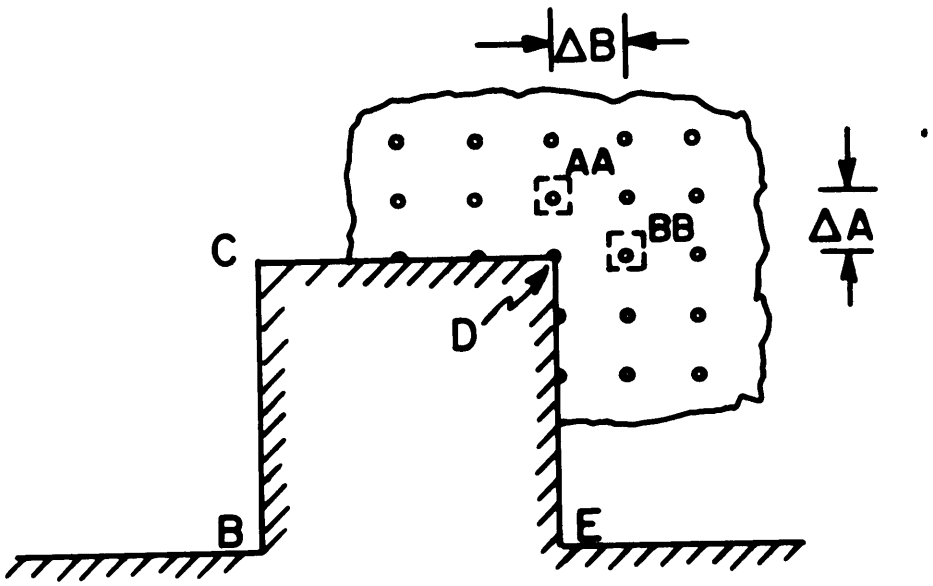

Figure B-1 Notation and Geometry for Vorticity at Sharp Corners

Points C and D can both be described in the same manner, so for sake of clarity let us confine our attention to the downstream corner D. If point D is considered part of the vertical wall DE, the first-order formulation for wall vorticity given by equation (A7) becomes

$$\zeta_D = -\frac{2}{(\Delta B)^2}\left[\psi_{BB} - \psi_D\right]. \tag{B1}$$

If point D is considered to lie on the horizontal wall CD, the first-order equation for wall vorticity becomes

$$\zeta_D = -\frac{2}{(\Delta A)^2}\left[\psi_{AA} - \psi_D\right]. \tag{B2}$$

Obviously, only in special cases would these two equations be equivalent. A similar set of equations results by using equation (A8) representing

the second-order formulation for wall vorticity;

$$\zeta_D = -\frac{3}{(\Delta B)^2}\left[\psi_{BB} - \psi_D\right] - \frac{\zeta_{BB}}{2}\,, \tag{B3}$$

and

$$\zeta_D = -\frac{3}{(\Delta A)^2}\left[\psi_{AA} - \psi_D\right] - \frac{\zeta_{AA}}{2}\,. \tag{B4}$$

Roache[3] suggests that both equations be used. If the first-order formulation for wall vorticity is being used, (B1) and (B2) would be employed in the following manner. When the grid scanning procedure reaches point AA just above point D, then ζ_D given by equation (B2) is used in the difference equations for AA. When ζ_D is required in the difference equations for point BB, equation (B1) is used. This technique for calculating the corner vorticity treats ζ as a double-valued function at the geometric singularity D. This is one of two techniques that have been employed in the present calculations. We refer to this as the double-valued technique. A similar procedure is employed with equations (B3) and (B4) if the second-order formulation is being used to calculate wall vorticity.

There are many other possibilities for treating the vorticity at the sharp convex corners. Roache and Mueller[9] have investigated seven different methods for treating the vorticity at the corner in a backstep-type geometry. Their conclusion is that at higher Reynolds numbers the calculated results are not very sensitive to the method used.

A second method was tested in our calculations in an attempt to force separation to occur at the sharp downstream corner D. This approach treats ζ_D as a single-valued function, assuming that the flow along wall CD determines the value of the vorticity at the corner. ζ_D is calculated using either equation (B2) or (B4), consistent with the procedure being used for the other wall points. This method will be referred to as the single-valued technique. Point C was treated as though it were on the downstream wall CD whenever the single-valued technique was used.

Our experience with these two methods showed that the results are sensitive to the technique used at low Reynolds numbers. The single-valued technique was not successful at forcing separation to occur at the downstream corner although the point of separation is very close to the corner--less than one cell below the corner.

DISTRIBUTION LIST

No. of Copies	Organization
12	Commander Defense Documentation Center ATTN: DDC-TCA Cameron Station Alexandria, Virginia 22314
1	Commander U.S. Army Materiel Command ATTN: AMCDL 5001 Eisenhower Avenue Alexandria, Virginia 22304
1	Commander U.S. Army Materiel Command ATTN: AMCRD, MG S. C. Meyer 5001 Eisenhower Avenue Alexandria, Virginia 22304
1	Commander U.S. Army Materiel Command ATTN: AMCRD, Dr.J.V.R.Kaufman 5001 Eisenhower Avenue Alexandria, Virginia 22304
1	Commander U.S. Army Materiel Command ATTN: AMCRD-T 5001 Eisenhower Avenue Alexandria, Virginia 22304
1	Commander U.S. Army Aviation Systems Command ATTN: AMSAV-E 12th and Spruce Streets St. Louis, Missouri 63166
1	Director U.S. Army Air Mobility Research and Development Laboratory Ames Research Center Moffett Field, California 94035
1	Commander U.S. Army Electronics Command ATTN: AMSEL-RD Fort Monmouth, New Jersey 07703
1	Commander U.S. Army Missile Command ATTN: AMSMI-R Redstone Arsenal, Alabama 35809
1	Commander U.S. Army Tank Automotive Command ATTN: AMSTA-RHFL Warren, Michigan 48090
2	Commander U.S. Army Mobility Equipment Research & Development Center ATTN: Tech Docu Cen, Bldg. 315 AMSME-RZT Fort Belvoir, Virginia 22060
1	Commander U.S. Army Armament Command Rock Island, Illinois 61202
1	Director U.S. Army Advanced Materiel Concepts Agency 2461 Eisenhower Avenue Alexandria, Virginia 22314
1	Commander U.S. Army Harry Diamond Laboratories ATTN: AMXDO-TI Washington, DC 20438

DISTRIBUTION LIST

No. of Copies	Organization
2	Director National Aeronautical and Space Administration Ames Research Center ATTN: Dr. F. R. Bailey Dr. J. M. Klineberg Moffett Field, CA 94035
2	Director National Aeronautical and Space Administration Langley Research Center ATTN: Dr. J. E. Carter Dr. S. F. Wornom Langley Station Hampton, VA 23365
	Aberdeen Proving Ground
	Ch, Tech Lib Marine Corps Ln Ofc Dir, USAMSAA

Unclassified

Security Classification

DOCUMENT CONTROL DATA - R & D

(Security classification of title, body of abstract and indexing annotation must be entered when the overall report is classified)

1. ORIGINATING ACTIVITY (Corporate author)	2a. REPORT SECURITY CLASSIFICATION
U.S. Army Ballistic Research Laboratories Aberdeen Proving Ground, Maryland 21005	Unclassified
	2b. GROUP

3. REPORT TITLE

SEPARATION AND REATTACHMENT NEAR SQUARE PROTUBERANCES IN LOW REYNOLDS NUMBER COUETTE FLOW

4. DESCRIPTIVE NOTES (Type of report and inclusive dates)

5. AUTHOR(S) (First name, middle initial, last name)

Clarence W. Kitchens, Jr.

6. REPORT DATE	7a. TOTAL NO. OF PAGES	7b. NO. OF REFS
JANUARY 1974	44	9

8a. CONTRACT OR GRANT NO.	9a. ORIGINATOR'S REPORT NUMBER(S)
b. PROJECT NO. RDT&E 1T061101A91A	BRL REPORT NO. 1695
c.	9b. OTHER REPORT NO(S) (Any other numbers that may be assigned this report)
d.	

10. DISTRIBUTION STATEMENT

Approved for public release; distribution unlimited.

11. SUPPLEMENTARY NOTES	12. SPONSORING MILITARY ACTIVITY
	U.S. Army Materiel Command 5001 Eisenhower Avenue Alexandria, Virginia 22304

13. ABSTRACT

Numerical solutions of the steady-state Navier-Stokes equations are obtained which describe flow past a square protuberance immersed in a plane Couette flow. The numerical solutions are illustrated with velocity vector plots, and plots of streamlines and vorticity contours in the flow field for Reynolds numbers between 1 and 200, based on plate velocity and protuberance height. A small separation bubble is predicted upstream of the protuberance with length and height almost independent of Reynolds number. The downstream separation bubble has a height always less than the protuberance height, but a length which increases almost linearly with Reynolds number reaching more than twenty-five protuberance heights at Re = 200. The flow perturbations caused by the protuberance are shown to persist far downstream of the protuberance at Re = 100 and 200.

DD FORM 1 NOV 68 1473 REPLACES DD FORM 1473, 1 JAN 64, WHICH IS OBSOLETE FOR ARMY USE.

Unclassified

Security Classification

14. KEY WORDS	LINK A		LINK B		LINK C	
	ROLE	WT	ROLE	WT	ROLE	WT
Navier-Stokes equations fluid dynamics separation reattachment protuberances low Reynolds number						